ChemPubSoc Europe

DOI: 10.1002/chem.201905241

CHEMISTRY
A European Journal
Communication

Luminescence |*Hot Paper*|

Iodinated Metallacrowns: Toward Combined Bimodal Near-Infrared and X-Ray Contrast Imaging Agents

Jacob C. Lutter,[a] Svetlana V. Eliseeva,*[b] Guillaume Collet,[b] Ivana Martinić,[b] Jeff W. Kampf,[a] Bernadette L. Schneider,[a] Aidan Carichner,[a] Julien Sobilo,[c] Stéphanie Lerondel,[c] Stéphane Petoud,*[b] and Vincent L. Pecoraro*[a]

Abstract: Multimodal probes capable of combining imaging modalities within a single molecule are in high demand today as they can provide information at both molecular and anatomical levels. Herein, a study was conducted on a series of gallium(III)/lanthanide(III) bis(12-MC-4) metallacrowns (MCs) with the general composition $\{Ln[12\text{-}MC_{Ga^{III}N(shi)}\text{-}4]\}_2(iph)_4$ (**Ln-I$_x$**, $x=0$, 4, 8, 12), where shi and iph are salicylhydroximate and isophthalate ligands, respectively, or their iodinated derivatives. For **Yb-I$_x$**, the attenuation in X-ray computed tomography (XCT) imaging and near-infrared (NIR) luminescence properties can be finely tuned by controlled structural modifications based on iodo groups. Solutions of **Yb-I$_x$** appear to be 22–40 times more efficient as XCT agents in comparison to the commercially available iobitridol, while providing an intense emission signal in the NIR range with total quantum yields up to 8.6%, which are among the highest values reported so far. Therefore, these molecules are promising potential bimodal agents for combined NIR luminescence and XCT imaging.

The need for the unambiguous and complete localization, identification and understanding of complex pathologies is exponentially growing in order to identify rapidly and with high accuracy the most efficient treatment. Multimodal imaging is attractive to achieve this specific goal by combining different imaging modalities to obtain complementary information at the anatomical, functional and molecular levels.[1–5] The key requirement is the availability of common probes able to operate in different imaging modalities. Among numerous imaging modalities, X-ray computed tomography (XCT) is an ideal anatomical imaging technique that allows the detailed visualization of organs and their contents. As a limitation, it does not provide molecular imaging with a sufficient resolution and sensitivity. On the other hand, fluorescence/luminescence imaging provides an excellent detection sensitivity at the molecular level and high cellular image resolution but offers limited anatomical information due to the scattering of the photons. In this respect, the creation of bimodal imaging agents suitable for both luminescence imaging and XCT appears to be highly advantageous.[6–8] Taking into account different sensitivities of XCT and optical imaging, our aim was to create bimodal probes which may balance this discrepancy by combining enhanced molar X-ray attenuation, that is, lowering the required concentration for effective XCT, with near-infrared (NIR) luminescence.

Metallacrowns (MCs), originally described as an inorganic structural analogues to crown ethers[9] have been employed in a wide array of research topics[10–21] including NIR optical imaging.[22,23] Several families of MCs have demonstrated an outstanding ability to protect and efficiently sensitize the characteristic emission of lanthanide(III) ions (Ln^{3+}) in the visible and in the NIR ranges.[24–28] Herein, we report a new series of gallium(III)/lanthanide(III) bis(12-MC-4) MCs with different iodine content, inspired by the success of iodinated small iodoorganic molecules such as iopamidol or iobitridol as CT contrast agents.[29,30] Three new scaffolds were created in which the iodine is introduced exclusively onto the H_2iph ($\{Ln[12\text{-}MC_{Ga^{III}N(shi)}\text{-}4]\}_2(iiph)_4$, **Ln-I$_4$**) or the H_3shi ($\{Ln[12\text{-}MC_{Ga^{III}N(mishi)}\text{-}4]\}_2(iph)_4$, **Ln-I$_8$**), or onto both ligand structures simultaneously ($\{Ln[12\text{-}MC_{Ga^{III}N(mishi)}\text{-}4]\}_2(iiph)_4$, **Ln-I$_{12}$**)) (Figure 1a). By leveraging these ligand substitutions, MCs with different iodine contents and locations were obtained, thus allowing one to follow and to control the effect of such modifications on the corresponding functional properties, that is, X-ray attenuation and NIR luminescence. Among the different luminescent Ln^{3+}, we focus our present studies on Yb^{3+} since this cation exhibits characteristic NIR emission in the 900–1100 nm range which lies within the biological diagnostic window.[31] For the sake of

[a] Dr. J. C. Lutter, Dr. J. W. Kampf, B. L. Schneider, A. Carichner, Prof. Dr. V. L. Pecoraro
Department of Chemistry, Willard H. Dow Laboratories
The University of Michigan
Ann Arbor, MI 48109 (United States)
E-mail: vlpec@umich.edu

[b] Dr. S. V. Eliseeva, Dr. G. Collet, Dr. I. Martinić, Prof. Dr. S. Petoud
Centre de Biophysique Moléculaire
CNRS UPR 4301
45071 Orléans Cedex 2 (France)
E-mail: svetlana.eliseeva@cnrs-orleans.fr
stephane.petoud@inserm.fr

[c] Dr. J. Sobilo, Dr. S. Lerondel
Centre d'Imagerie du Petit Animal
PHENOMIN-TAAM
45071 Orléans Cedex 2 (France)

Supporting information (including experimental details, synthetic procedures, physical methods, detailed description of photophysical measurements, and XCT attenuation parameters) and the ORCID identification number(s) for the author(s) of this article can be found under: https://doi.org/10.1002/chem.201905241.

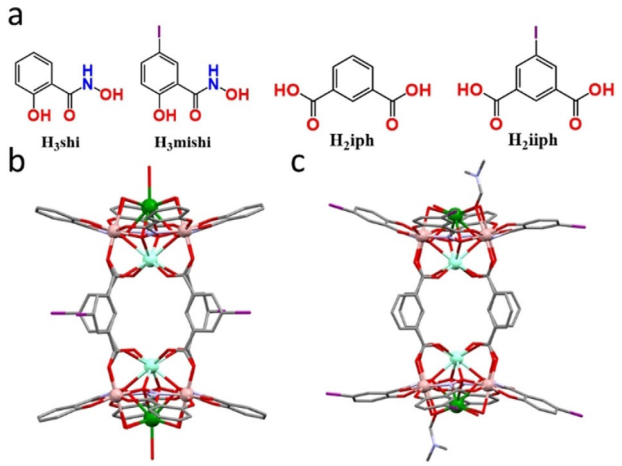

Figure 1. (a) Structural formulas of the hydroxamic acids (H_3shi, H_3mishi) and the bridging ligands (H_2iph, H_2iiph). Crystallographic structures of (b) **Sm-I$_4$** and (c) **Sm-I$_8$**. Sm: cyan; Ga: rose; O: red; N: light blue; C: grey; I: purple; Na: green. The hydrogen atoms and solvent molecules have been omitted for clarity.

comparison, the $\{Ln[12\text{-}MC_{Ga}{}^{III}{}_{N(shi)}\text{-}4]\}_2(iph)_4$ (**Ln-I$_0$**) MC with Na^+ as a counter-cation was synthesized, as the previously reported structure contained NH_4^+.[27] Crystallographic models of **Sm-I$_4$** and **Sm-I$_8$** are shown in Figures 1b and 1c. Both molecules exhibit a dimeric structure where Sm[12-MC-4] motifs are linked together by bridging isophthalate derivatives. A full analysis of these structures can be found in the Supporting Information. CCDC 1970092, 1970093 contain the supplementary crystallographic data for this paper. These data are provided free of charge by The Cambridge Crystallographic Data Centre.

With respect to the ligand-centered photophysical properties, the iodination of the isophthalate has a limited impact while that of the salicylhydroximate results in the red shift of the absorption (Figure 2a) and emission bands. Thus, low-energy absorption bands of **Yb-I$_0$** and **Yb-I$_4$** lie in the range of 290–355 nm (λ_{max}: 317–318 nm, ε: $\approx 5\times10^4$ M^{-1} cm^{-1}), while these of **Yb-I$_8$** and **Yb-I$_{12}$** are observed at 300–370 nm (λ_{max}: $\approx$335 nm, ε: $\approx 4.1\times10^4$ M^{-1} cm^{-1}). The energies of the singlet (S_1) electronic states estimated from the edges of the absorption spectra are 28170 cm^{-1} for **Yb-I$_0$** and **Yb-I$_4$**, and 27030 cm^{-1} for **Yb-I$_8$** and **Yb-I$_{12}$**. To obtain information about the energy positions of the triplet (T_1) states, that are assumed to play an important role in the sensitization of Ln^{3+} emission,[32] phosphorescence spectra of **Gd-I$_x$** (x=0, 4, 8, 12) were acquired in the solid state (Figure S15). They showed resolved vibronic structure for the 0–0, 0–1 and 0–2 transitions with progression of 1275–1570 cm^{-1} (Table S2). The corresponding T_1 energies estimated as being 0–0 transitions are located at 22385 and 22130 cm^{-1} for **Gd-I$_0$** and **Gd-I$_4$**, 21780 and 21730 cm^{-1} for **Gd-I$_8$** and **Gd-I$_{12}$**.

Yb^{3+}-centered photophysical properties were studied for the new **Yb-I$_x$** in solution and in the solid state (Figure 2b, Table 1 and S3). Excitation spectra collected upon monitoring the Yb^{3+} emission at 980 nm exhibit broad bands in the range 250–450 nm. As the Yb^{3+} cation does not possess electronic levels in this domain, the only way to sensitize its emission using

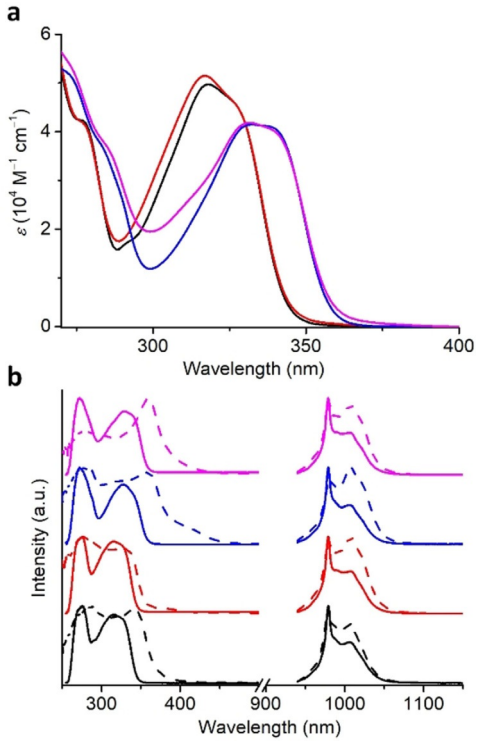

Figure 2. (a) Absorption spectra in solution (50 μM, DMF), and (b) corrected and normalized (left) excitation (λ_{em}=980 nm) and (right) emission (λ_{ex}=320–350 nm) spectra collected in the solid state (dashed traces) and in solution (50 μM, DMF; solid traces) of **Yb-I$_x$** MCs (x=0, 4, 8, 12) at room temperature. Black : **Yb-I$_0$**; red : **Yb-I$_4$**; blue : **Yb-I$_8$**; magenta : **Yb-I$_{12}$**.

Table 1. Photophysical parameters of **Yb-I$_x$** in solution (50 μM, DMF) at room temperature.[a]

Yb-I$_x$	τ_{obs} [μs][b]	τ_{rad} [μs][c]	Q_{Yb}^{Yb} [%][d]	Q_{Yb}^{L} [%][e]	η_{sens} [%][f]
Yb-I$_0$	51.1(2)	295	17	8.6(1)	51
Yb-I$_4$	51.3 (1)	230	22	8.32(4)	37.8
Yb-I$_8$	50(2)	270	18	4.5(1)	25
Yb-I$_{12}$	51(1)	170	30	4.13(8)	13.8

[a] 2σ values within parentheses. Relative errors: τ_{obs}, ±2%; Q_{Yb}^{L}, ±10%; τ_{rad}, ±10%; Q_{Yb}^{Yb}, ±12%; η_{sens}, ±22%. [b] λ_{ex}=355 nm. [c] From absorption spectra using Eq. (S1a, S1b). [d] From Eq. (1) and (S2). [e] λ_{ex}=320 nm for **Yb-I$_0$**, **Yb-I$_4$**, or 335 nm for **Yb-I$_8$**, **Yb-I$_{12}$**. [f] From Eq. (1) and (S3).

such excitation wavelengths is through the "antenna effect".[33] Upon excitation of **Yb-I$_x$** at 320–350 nm, intense Yb^{3+} emission bands arising from the $^2F_{5/2}\rightarrow{}^2F_{7/2}$ transition were observed. These results confirm that the MCs scaffolds of the **Yb-I$_x$** are suitable for the sensitization of the NIR Yb^{3+} emission although with different sensitization efficiencies, η_{sens}.

Indeed, the global process of the Yb^{3+} sensitization through the "antenna effect" can be described by Equation (1):[32]

$$Q_{Yb}^{L} = \eta_{sens} \times Q_{Yb}^{Yb} = \eta_{sens} \times \frac{\tau_{obs}}{\tau_{rad}} \quad (1)$$

where Q_{Yb}^{L} and Q_{Yb}^{Yb} are, respectively the total (under ligand excitation) and the intrinsic quantum yields of Yb^{3+}-centered

emission; τ_{obs} and τ_{rad} are the observed and the radiative lifetimes. Following Eq. (1), η_{sens} can be calculated as the ratio between Q^{L}_{Yb} and Q^{Yb}_{Yb}. However, if Q^{L}_{Yb} can be experimentally measured by an absolute method using an integration sphere as[34] the experimental determination of Q^{Yb}_{Yb} is limited because of the extremely low molar absorption coefficients of f-f transitions. Alternatively, Q^{Yb}_{Yb} can be estimated as the ratio between τ_{obs} and τ_{rad}. The τ_{obs} can be easily measured experimentally, but the determination of the τ_{rad} is not as straightforward. However, in the case of Yb^{3+}, electronic transitions generating the NIR luminescence terminate onto the ground level, so that absorption spectra in the range of the $^2F_{5/2} \leftarrow {}^2F_{7/2}$ transition can be acquired (Figure S21) and used to estimate the corresponding τ_{rad}. Having all these experimental parameters in hand, Q^{Yb}_{Yb} and η_{sens} can be quantified.

Observed lifetime values of 50–51 μs for **Yb-I$_x$** in solution are the same within experimental error, reflecting the similarity of coordination environments around Yb^{3+} and the corresponding levels of protection provided by the MCs scaffolds. On the other hand, τ_{rad} values are being reduced from 295 to 230, 270 and 170 μs when going from **Yb-I$_0$** to **Yb-I$_4$**, **Yb-I$_8$** and **Yb-I$_{12}$**. Therefore, the increase of the iodine content most probably induces a larger mixing of the electronic states of the ligands with the Yb^{3+} f-orbitals inducing the $^2F_{5/2} \rightarrow {}^2F_{7/2}$ transition to be less forbidden.[35] In turn, the shortening of τ_{rad} results in an increase of Q^{Yb}_{Yb} values from 17% for **Yb-I$_0$** to 30% for **Yb-I$_{12}$**. Nevertheless, Q^{L}_{Yb} values that are directly related to Q^{Yb}_{Yb} are 1.8–2.1 times lower for **Yb-I$_8$** and **Yb-I$_{12}$** compared to **Yb-I$_0$** and **Yb-I$_4$** as a result of a gradual decrease of sensitization efficiencies upon iodination from 51 to 13.8%. The negative effect of the iodination of isophthalate ligands on η_{sens} when going from **Yb-I$_0$** to **Yb-I$_4$** could be compensated by the 1.3 times shortening of τ_{rad} value, so that the Q^{L}_{Yb} values remain the same within experimental errors for these two MCs, 8.3–8.6%. A similar situation is occurring for **Yb-I$_8$** and **Yb-I$_{12}$**. It should be noted that η_{sens} are significantly impacted within the studied series of **Yb-I$_x$** despite the fact that the T_1 energies lie within a very narrow range (21 730–22 385 cm^{-1}).

The analysis of quantitative parameters and their rationalization with the iodine content for **Yb-I$_x$** in the solid state is less straightforward (Table S3). In general, quantum yields, η_{sens} and τ_{obs} are lower for the solid state samples compared to the corresponding values in solution. Such behavior most probably reflects the existence of additional and/or more efficient non-radiative processes induced by intermolecular interactions present in the solid state compared to the sole interactions with solvent molecules when MCs are discrete species dispersed in the solution. We should also point out that the role of the counter-cation cannot be neglected as τ_{obs} and Q^{L}_{Yb} values measured for **Yb-I$_0$** (Na^+ counter-cation) in the solid state are significantly larger than in the case of the previously published analogues isolated with NH_4^+ as a counter-cation,[27] that is, 37.1 μs and 4.8% vs. 30.5 μs and 2.4%.

X-ray attenuation experiments were carried out on solutions of **Yb-I$_x$** with different concentrations (Figure 3a). The volume X-ray attenuation (HU μL^{-1}) was estimated for each sample (see Supporting Information) and a linear dependence with the concentration was demonstrated (Figure 3b). The slope of this dependence reflects the molar radiodensity and gives values of molar X-ray attenuation coefficients (HU_m) of 8.82, 11.72, 14.10 and 17.62 HU mmol^{-1} for **Yb-I$_0$**, **Yb-I$_4$**, **Yb-I$_8$**, **Yb-I$_{12}$**, respectively. These values are 23–46 times superior to the one (0.38 HU mmol^{-1}) calculated for the commercially available XCT contrast agent iobitridol using the same experimental procedure.

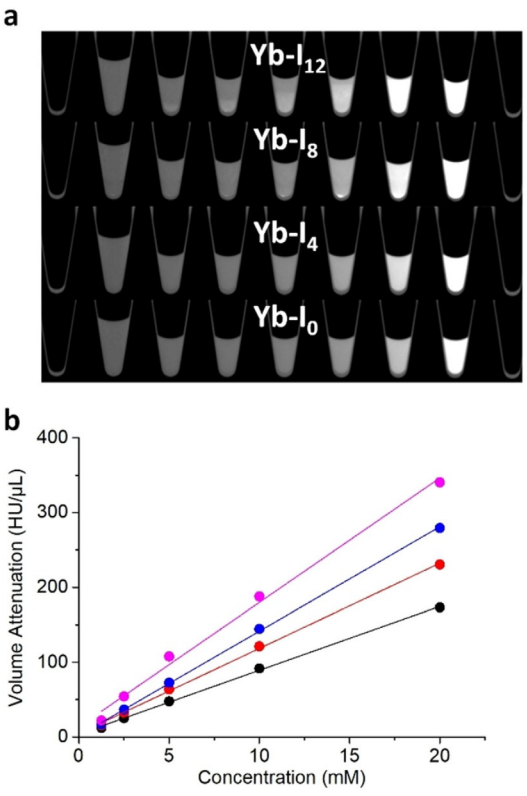

Figure 3. (a) XCT images of solutions of **Yb-I$_x$** in DMF (from right to left : 20 mM, 10 mM, 5 mM, 2.5 mM, 1.25 mM, 625 μM and 312.5 μM). (b) MC's volume attenuation (HU μL^{-1}) vs. concentration. Black : **Yb-I$_0$**; red : **Yb-I$_4$**; blue : **Yb-I$_8$**; magenta : **Yb-I$_{12}$**.

In conclusion, we have created here a new series of gallium(III)/ytterbium(III) bis(12-MC-4) MCs (**Yb-I$_x$**, $x = 0$, 4, 8, 12) in which NIR luminescent properties and X-ray attenuation can be tuned through the controlled iodination of either isophthalate and/or salicylhydroximate ligands. A high density of elements with large Z in the studied series of MCs induces a significant XCT attenuation reaching a value of 17.62 HU mmol^{-1} for **Yb-I$_{12}$**, while the presence of Yb^{3+} results in a highly intense NIR emission with total quantum yields up to 8.6% in solution, among the highest values reported to date for NIR-emitting lanthanide(III) compounds. In respect to the photostability of these MCs, we have observed that **Yb-I$_x$** can release iodine upon UV illumination (see Supporting Information). The stability of C–I bonds should not be neglected since this phenomenon is known to occur in several other iodoorganic molecules.[36,37] These competing observations suggest that the **Yb-I$_4$** represents an attractive compromise with the maximization of the NIR emission intensity and of the X-ray contrast efficien-

cy while diminishing the C–I photoinstability. It also suggests that these compounds are highly promising candidates for the creation of bimodal agents suitable for combined NIR luminescence and XCT imaging.

Acknowledgements

The work was supported through grants from the National Science Foundation (CHE 1664964 for J.C.L. and V.L.P., CHE 0840456 for J.W.K.), La Ligue Régionale Contre le Cancer and La Région Centre Val de Loire. G.C. and I.M. acknowledge the support from the University of Orléans. S.P. thanks Institut National de la Santé et de la Recherche Médicale.

Conflict of interest

The authors declare no conflict of interest.

Keywords: lanthanides · luminescence · metallacrowns · near-infrared · X-ray computed tomography

[1] A. Louie, *Chem. Rev.* **2010**, *110*, 3146 – 3195.
[2] B. R. Smith, S. S. Gambhir, *Chem. Rev.* **2017**, *117*, 901 – 986.
[3] K. Heinzmann, L. M. Carter, J. S. Lewis, E. O. Aboagye, *Nat. Biomed. Eng.* **2017**, *1*, 697 – 713.
[4] X. Li, X.-N. Zhang, X.-D. Li, J. Chang, X. Li, X.-N. Zhang, X.-D. Li, J. Chang, *Cancer Biol. Med.* **2016**, *13*, 339 – 348.
[5] B. P. Burke, C. Cawthorne, S. J. Archibald, *Philos. Trans. R. Soc. London Ser. A* **2017**, *375*, 20170261.
[6] H. Xing, W. Bu, Q. Ren, X. Zheng, M. Li, S. Zhang, H. Qu, Z. Wang, Y. Hua, K. Zhao, L. Zhou, W. Peng, J. Shi, *Biomaterials* **2012**, *33*, 5384 – 5393.
[7] R. Meenambal, S. Kannan, *Mater. Sci. Eng. C* **2018**, *91*, 817 – 823.
[8] D. González-Mancebo, A. I. Becerro, T. C. Rojas, A. Olivencia, A. Corral, M. Balcerzyk, E. Cantelar, F. Cussó, M. Ocaña, *J. Colloid Interface Sci.* **2018**, *520*, 134 – 144.
[9] M. S. Lah, V. L. Pecoraro, *J. Am. Chem. Soc.* **1989**, *111*, 7258 – 7259.
[10] J. C. Lutter, C. M. Zaleski, V. L. Pecoraro in *Supramolecular Chemistry. Advances in Inorganic Chemistry, Vol. 71* (Eds.: R. van Eldik, R. Puchta), Elsevier, Cambridge, **2018**, pp. 177 – 246.
[11] C. Sgarlata, A. Giuffrida, E. R. Trivedi, V. L. Pecoraro, G. Arena, *Inorg. Chem.* **2017**, *56*, 4771 – 4774.
[12] M. A. Katkova, G. S. Zabrodina, M. S. Muravyeva, A. A. Khrapichev, M. A. Samsonov, G. K. Fukin, S. Y. Ketkov, *Inorg. Chem. Commun.* **2015**, *52*, 31 – 33.
[13] T. N. Parac-Vogt, A. Pacco, P. Nockemann, S. Laurent, R. N. Muller, M. Wickleder, G. Meyer, L. Vander Elst, K. Binnemans, *Chem. Eur. J.* **2006**, *12*, 204 – 210.
[14] C. M. Zaleski, C.-S. Lim, A. D. Cutland-Van Noord, J. W. Kampf, V. L. Pecoraro, *Inorg. Chem.* **2011**, *50*, 7707 – 7717.
[15] T. T. Boron, J. W. Kampf, V. L. Pecoraro, *Inorg. Chem.* **2010**, *49*, 9104 – 9106.
[16] T. T. Boron III, J. C. Lutter, C. I. Daly, C. Y. Chow, A. H. Davis, A. Nimthong-Roldán, M. Zeller, J. W. Kampf, C. M. Zaleski, V. L. Pecoraro, *Inorg. Chem.* **2016**, *55*, 10597 – 10607.
[17] C. M. Zaleski, E. C. Depperman, J. W. Kampf, M. L. Kirk, V. L. Pecoraro, *Inorg. Chem.* **2006**, *45*, 10022 – 10024.
[18] C. Y. Chow, H. Bolvin, V. E. Campbell, R. Guillot, J. W. Kampf, W. Wernsdorfer, F. Gendron, J. Autschbach, V. L. Pecoraro, T. Mallah, *Chem. Sci.* **2015**, *6*, 4148 – 4159.
[19] C. Y. Chow, R. Guillot, E. Rivière, J. W. Kampf, T. Mallah, V. L. Pecoraro, *Inorg. Chem.* **2016**, *55*, 10238 – 10247.
[20] A. J. Stemmler, J. W. Kampf, M. L. Kirk, B. H. Atasi, V. L. Pecoraro, *Inorg. Chem.* **1999**, *38*, 2807 – 2817.
[21] M. S. Muravyeva, G. S. Zabrodina, M. A. Samsonov, E. A. Kluev, A. A. Khrapichev, M. A. Katkova, I. V. Mukhina, *Polyhedron* **2016**, *114*, 165 – 171.
[22] I. Martinić, S. V. Eliseeva, T. N. Nguyen, F. Foucher, D. Gosset, F. Westall, V. L. Pecoraro, S. Petoud, *Chem. Sci.* **2017**, *8*, 6042 – 6050.
[23] I. Martinić, S. V. Eliseeva, T. N. Nguyen, V. L. Pecoraro, S. Petoud, *J. Am. Chem. Soc.* **2017**, *139*, 8388 – 8391.
[24] E. R. Trivedi, S. V. Eliseeva, J. Jankolovits, M. M. Olmstead, S. Petoud, V. L. Pecoraro, *J. Am. Chem. Soc.* **2014**, *136*, 1526 – 1534.
[25] C. Y. Chow, S. V. Eliseeva, E. R. Trivedi, T. N. Nguyen, J. W. Kampf, S. Petoud, V. L. Pecoraro, *J. Am. Chem. Soc.* **2016**, *138*, 5100 – 5109.
[26] J. C. Lutter, S. V. Eliseeva, J. W. Kampf, S. Petoud, V. L. Pecoraro, *Chem. Eur. J.* **2018**, *24*, 10773 – 10783.
[27] T. N. Nguyen, C. Y. Chow, S. V. Eliseeva, E. R. Trivedi, J. W. Kampf, I. Martinić, S. Petoud, V. L. Pecoraro, *Chem. Eur. J.* **2018**, *24*, 1031 – 1035.
[28] J. Jankolovits, C. M. Andolina, J. W. Kampf, K. N. Raymond, V. L. Pecoraro, *Angew. Chem. Int. Ed.* **2011**, *50*, 9660 – 9664; *Angew. Chem.* **2011**, *123*, 9834 – 9838.
[29] H. Lusic, M. W. Grinstaff, *Chem. Rev.* **2013**, *113*, 1641 – 1666.
[30] P. J. Fournier, W. Steinbrich, P. Freitag, E. Voegeli, *Eur. J. Radiol.* **1996**, *23*, 185 – 189.
[31] I. Martinić, S. V. Eliseeva, S. Petoud, *J. Lumin.* **2017**, *189*, 19 – 43.
[32] J.-C. G. Bünzli, S. V. Eliseeva in *Comprehensive Inorganic Chemistry II,* Elsevier, Amsterdam **2013**, pp. 339 – 398.
[33] H. Uh, S. Petoud, *Comptes Rendus Chim.* **2010**, *13*, 668 – 680.
[34] H. Ishida, J.-C. Bünzli, A. Beeby, *Pure Appl. Chem.* **2016**, *88*, 701 – 711.
[35] J.-C. G. Bünzli, A. S. Chauvin, H. K. Kim, E. Deiters, S. V. Eliseeva, *Coord. Chem. Rev.* **2010**, *254*, 2623 – 2633.
[36] E. Grönewäller, H. Wahl, R. Kehlbach, H. Rodemann, C. Claussen, S. Duda, *Fortschr. Röntgenstr.* **1998**, *169*, 537 – 541.
[37] L. Cavina, D. van der Born, P. H. M. Klaren, M. C. Feiters, O. C. Boerman, F. P. J. T. Rutjes, *Eur. J. Org. Chem.* **2017**, 3387 – 3414.

Manuscript received: November 19, 2019
Accepted manuscript online: December 6, 2019
Version of record online: January 21, 2020